

See discussions, stats, and author profiles for this publication at: <https://www.researchgate.net/publication/277601799>

Bacteria-Targeting Conjugates Based on Antimicrobial Peptide for Bacteria Diagnosis and Therapy

ARTICLE *in* MOLECULAR PHARMACEUTICS · JUNE 2015

Impact Factor: 4.38 · DOI: 10.1021/acs.molpharmaceut.5b00053 · Source: PubMed

READS

53

8 AUTHORS, INCLUDING:



Haiyan Chen

China Pharmaceutical University

51 PUBLICATIONS 622 CITATIONS

[SEE PROFILE](#)



Xinyue Dong

Washington State University

3 PUBLICATIONS 0 CITATIONS

[SEE PROFILE](#)



Yueqing Gu

China Pharmaceutical University

124 PUBLICATIONS 1,471 CITATIONS

[SEE PROFILE](#)

Bacteria-Targeting Conjugates Based on Antimicrobial Peptide for Bacteria Diagnosis and Therapy

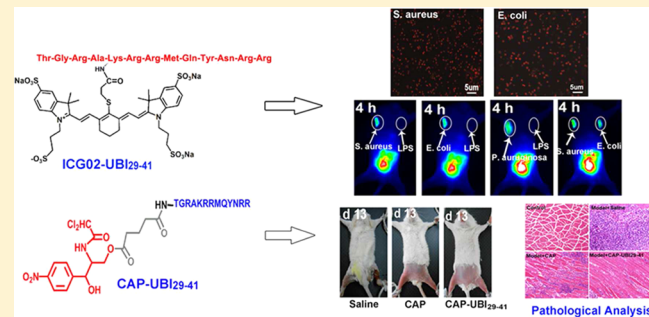
Haiyan Chen,[†] Cuicui Liu,[†] Dan Chen,[†] Kyle Madrid,[§] Shuwen Peng,[†] Xinyue Dong,[‡] Min Zhang,[†] and Yueqing Gu^{*,†}

[†]Department of Biomedical Engineering, School of Engineering, State Key Laboratory of Natural Medicines, and [‡]School of Pharmacy, China Pharmaceutical University, 24 Tongjia Lane, Gulou District, Nanjing 210009, China

[§]Department of Chemistry, University of California, 900 University Avenue, Riverside, California 92521, United States

ABSTRACT: Chloramphenicol (CAP) is one of the most effective antimicrobial agents, but its therapeutic efficacy is greatly limited by its nonspecific distribution and consequent side effects in neutrophils. Targeting to the infection sites, and thus restricting CAP nonselective delivery, provides an alternative way to overcome this limitation. The antibacterial peptide fragment UBI_{29–41} was identified to have a high bacterial affinity. However, no research so far has been carried out to utilize UBI_{29–41} as a ligand for bacteria-targeting therapies. In this Article, we first labeled a near-infrared fluorescent dye (ICG02) with UBI_{29–41} to investigate its targeting capability in different bacteria (*S. aureus*, *E. coli*, and *P. aeruginosa*) and bacteria-infected mouse models. Subsequently, UBI_{29–41} was conjugated with the typical antibiotic (CAP) through the linker glutaric anhydride to form the conjugate CAP-UBI_{29–41} for the bacteria-targeting therapy. *In vitro* studies demonstrated the enhanced antibacterial effects of CAP-UBI_{29–41} on *S. aureus* and *E. coli*. Meanwhile, the toxicity of CAP-UBI_{29–41} on normal cells decreased distinctly in comparison with CAP. Most importantly, CAP-UBI_{29–41} exhibited more favorable antibacterial efficacy than CAP in bacteria-bearing mouse models. All these results demonstrated that UBI_{29–41} is an ideal targeting ligand to construct antibacterial agents for bacteria-targeting therapy.

KEYWORDS: chloramphenicol, UBI_{29–41}, bacteria-targeting, diagnosis, therapy



1. INTRODUCTION

Despite the availability of various antibiotics, bacterial infections are still a major cause of mortality and morbidity worldwide as it is depicted in the statistics of the United States of America, where they cause high mortality from sepsis and are also the leading cause of limb amputations.^{1,2} The diagnostic approaches and therapeutic schemes to control the infection are mainly challenged by the increasing presence of tuberculosis and multidrug resistant bacteria.³ Therefore, a rapid and accurate identification method for bacterial infections is critical for authentic anti-infective therapy. Traditionally, only infections that have become systemic or have caused significant anatomical tissue damages⁴ could be diagnosed using several inconvenient and time-consuming methods including laboratory culture tests,⁵ nuclear medicine imaging,⁶ and computed tomography (CT).^{7,8} Hence, many researchers have switched to the direction of designing bacteria-targeting probes with tissue-selective ligands, e.g., antibodies, lectin, sugar, etc.,^{9,10} to improve the bacterial diagnosis.^{11,12} A more effective approach to achieve broad bacteria-targeting has been utilized in nanoparticle surface modifications, ligand–acceptor interactions, and so on.^{13–15} For example, cationic molecules on the surface of nanoparticles can be electrostatically attracted by the negatively

charged bacteria, which are attributed to the high fraction of anionic phospholipids and amphiphile molecules.^{16,17}

UBI_{29–41}, a cationic human antimicrobial peptide fragment (MW 1.69 kDa) with six positively charged residues (5 Arg + 1 Lys), was recently used to label technetium-99m (^{99m}Tc), and the probe was widely investigated for its capacity to bind bacteria.^{18,19} In clinical trials, ^{99m}Tc-UBI_{29–41} demonstrated the detection of bacterial infection with high sensitivity, specificity, and accuracy. Near infrared (NIR) imaging, which possesses the merits of nonradioactivity and deep tissue penetration ability, has emerged as a powerful tool for disease diagnosis.^{20–22} To this day, few investigations were performed on *in vivo* bacteria diagnosis by coupling NIR fluorescence imaging with bacteria-targeting contrast agents, which motivated us to carry out this research.

In this work, UBI_{29–41} was coupled to a deep tissue penetrating NIR agent and the resulting bacteria imaging probe was investigated both *in vitro* and *in vivo*. UBI_{29–41} was then conjugated to chloramphenicol (CAP), a prototypical

Received: January 18, 2015

Revised: May 20, 2015

Accepted: June 1, 2015

broad-spectrum antibiotic,²³ to overcome the nonspecificity and biotoxicity of CAP, which was verified in different bacteria and bacteria-bearing mouse models.

2. EXPERIMENTAL SECTION

2.1. Materials. UBI_{29–41} was obtained from China Peptides Technology Co. Ltd. CAP (MW 323.129) was purchased from Sigma-Aldrich (Shanghai, China). Glutaric anhydride (MW 114.1) was purchased from Sinopharm. ICG-Der-02 (abbreviated as ICG02, MW 995) was prepared in our laboratory.^{24,25} All other solvents and reagents used in this study were certified analytical reagent grade (Shanghai Chemical Reagent Company, Shanghai, China).

2.2. Synthesis and Characterization of ICG02-UBI_{29–41}. ICG02-UBI_{29–41} was synthesized according to a previous report.²⁶ In detail, ICG02 (5.0 mg, 0.005 mmol) was first reacted with EDC·HCl (2.0 mg, 0.01 mmol) and NHS (1.0 mg, 0.01 mmol) in anhydrous *N,N*-dimethylformamide (DMF, 0.2 mL). After stirring in the dark for 6 h at room temperature, the solution was mixed with UBI_{29–41} (3.0 mg, 0.002 mmol) in PBS buffer (2.0 mL). The mixture was stirred in the dark overnight at room temperature. The final product ICG02-UBI_{29–41} was identified by thin layer chromatography (TLC). After the reaction, the crude product ICG02-UBI_{29–41} was subsequently separated from free ICG02 and UBI_{29–41} by preparative HPLC (Waters 152S, USA). The absorption spectrum of ICG02-UBI_{29–41} was measured by UV-vis spectrometer. The fluorescence spectrum was measured at room temperature using an S2000 eight-channel optical fiber spectrofluorometer (Ocean Optics Corporation, USA) equipped with a xenon lamp ($\lambda = 765.9$ nm, Enlight, China). ICG02-UBI_{29–41} was further characterized by ¹H NMR and ¹³CNMR (Varian, USA). The EI-MS were recorded on a MAT-112-S machine at 70 eV. FT-IR spectra were recorded on a Bruker FT-IR Tensor 37 Spectrometer in the 4000–550 cm^{−1}. All the characterizations were repeated for the three times.

ICG02-UBI_{29–41}: ¹HNMR (D₂O, 400 MHz, δ ppm) 9.2–8.1 (s, 1 H, −NH−C=O), 7.8–6.6 (dd, 6 H, 6 H of benzene), 5.3–6.5 (s, 4 H, 4 H of ethylene), 3.5 (t, 4 H, −CH₂−SO₃Na), 3.15 (t, 2 H, −CH₂−S), 2.9 (t, 2 H, −CH₂−C=O), 2.8 (s, 1 H, OH); ¹³CNMR (D₂O, 75 MHz, δ ppm) 23.1, 24.6, 25.1, 27.4, 38.5, 43.7, 50.2, 52.1, 113.1, 116.5, 126.4, 130.6, 135.9, 140.3, 143.2, 145.7, 168.4, 169.5, 170.5, 172.3, 174.3, 175.3, 176.8; MS (EI) m/z (%) = 2666 [M⁺].

2.3. Synthesis and Characterization of CAP-UBI_{29–41}. O-Glutaryl-chloramphenicol (CAP-Glu) was prepared according to the following method. Briefly, CAP (2.0 g, 6.2 mmol) and glutaric anhydride (0.8 g, 6.82 mmol) were dissolved in dry tetrahydrofuran (THF). Then triethyl-amine (1.0 mL, 6.82 mmol) and dimethylamino pyridine (DMAP, 0.2 mL) were added. The mixture was stirred at room temperature overnight and monitored by thin-layer chromatography (TLC). The reaction mixture was diluted with ethyl acetate and washed by hydrochloric acid (HCl, 1.0 equiv). The organic layer was dried over magnesium sulfate, and the solvent was removed under reduced pressure. The crude product was purified by filtration through a silica gel column containing the solvents ethyl acetate and hexane. Fractions containing CAP-Glu were collected and concentrated under vacuum to obtain the yellow solid (2.1 g). The purified Glu-CAP was obtained with a yield of 51.8%. Finally, the molecular weight of the purified CAP-Glu was determined by LC-MS.

UBI_{29–41} (55.0 mg, 32 μ mol) was reacted with CAP-Glu (17.0 mg, 37 μ mol) in DMF (1.0 mL) according to Tulla-Puche's report.²⁷ HCTU (15.0 mg, 37 μ mol) and HOBr (4.9 mg, 37 μ mol) in DIPEA (12.1 μ L, 70 μ mol) were added. The reaction mixture was stirred for 6 h at room temperature. Then the supernatant was removed, and the residual oil was treated with ethyl acetate to obtain a white solid with 80% yield. Finally, the compound was purified by preparative HPLC and verified by ¹H NMR, ¹³CNMR, and ESI-MS. All the characterizations were repeated three times.

CAP-Glu: MS (EI) m/z (%) = 437.2. CAP-UBI_{29–41}: ¹HNMR (D₂O, 400 MHz, δ ppm) 8.1–7.4 (dd, 4 H, 4 H of benzene), 8.0 (s, 1 H, −NH−C=O), 6.4 (s, 1 H, −CHCl₂), 5.6 (d, 1 H, benzyl group), 4.7 (t, 4 H, −CH₂−SO₃Na), 4.3 (d, 2 H, −CH₂−O−), 2.3–2.5 (t, 2 H, −CH₂−C=O), 2.7 (s, 1 H, OH); ¹³CNMR (D₂O, 75 MHz, δ ppm) 21.2, 24.6, 25.1, 26.8, 27.4, 32.5, 38.5, 54.2, 65.1, 74.3, 76.4, 123.4, 128.5, 144.9, 160.3, 164.5, 171.3, 173.2, 174.2, 175.3; MS (EI) m/z (%) = 2110.3 [M⁺].

2.4. In Vitro Cytotoxicity of ICG02-UBI_{29–41} and CAP-UBI_{29–41}. The cytotoxicity of ICG02-UBI_{29–41} and CAP-UBI_{29–41} against different cell lines (L-02, HBL-100, and HELF) was investigated using the MTT assay following the standard protocols. Five independent MTT assays were performed for *in vitro* cytotoxicity evaluation. Briefly, cells were cultured in RPMI1640 medium with 10% FBS at 37 °C in the presence of 5% CO₂. The cells harvested at the logarithmic growth phase were plated into 96-well plates at a cell density of 5 × 10³ cells/well. After 24 h, ICG02-UBI_{29–41} and CAP-UBI_{29–41} with different concentrations (1.0 to 250 μ M) were added into the cells and incubated for 48 h. After MTT (20 μ L of 5 mg/mL) was subsequently incubated with the cells for 4 h, the medium containing MTT was carefully removed from each well, and 150 μ L of DMSO was added to dissolve the formed crystals. The percentage of cell viability was measured with a multiwell plate reader at 570 nm. The cell viability was calculated as follows:

$$\text{viable cell}(\%) = \frac{\text{OD}_{\text{treated}} - \text{OD}_{\text{media control}}}{\text{OD}_{\text{untreated}} - \text{OD}_{\text{media control}}} \times 100\%$$

where OD_{treated} was the absorbance obtained from ICG02-UBI_{29–41} incubated cells; OD_{untreated} was obtained from PBS incubated cells; and OD_{media control} was obtained from the blank medium incubated cells.

2.5. In Vitro Evaluation of the Antibacterial Activity of ICG02-UBI_{29–41}. *S. aureus* and *E. coli* cultured in LB broth were transferred into 5 mL of the growth medium respectively to grow overnight at 37 °C. Bacteria were centrifuged (8000 r/min) and resuspended in aqueous solutions with different pHs (5.5–7.5). The dynamic light scattering analyzer (Zetasizer 3000HSA, Malvern, Japan) was utilized to measure the zeta potentials of *S. aureus* and *E. coli* solutions. The zeta potential assay was repeated five times.

The antibacterial activity of ICG02-UBI_{29–41} was investigated in four different bacteria (*S. aureus*, *E. coli*, *P. aeruginosa*, and *B. subtilis*) by the broth microdilution method ($n = 5$). Briefly, 100 μ L of ICG02-UBI_{29–41} solutions with different concentrations (from 1.0 to 32.0 μ mol/L) was placed into the 96-well plates. One hundred microliters of bacteria solution (OD₆₀₀ = 0.3) was added to each well. The plates were incubated at 37 °C for 20 h. The survival rate of bacteria was measured at

600 nm using a multiwell plate reader and was calculated according to the following equation:

$$\text{survival rate}(\%) = \frac{\text{OD}_{\text{treated}} - \text{OD}_{\text{media control}}}{\text{OD}_{\text{untreated}} - \text{OD}_{\text{media control}}} \times 100\%$$

where $\text{OD}_{\text{treated}}$ was the absorbance obtained from ICG02-UBI₂₉₋₄₁ incubated bacteria; $\text{OD}_{\text{untreated}}$ was obtained from PBS incubated bacteria; and $\text{OD}_{\text{media control}}$ was obtained from the blank medium incubated bacteria.

2.6. In Vitro Evaluation of the Bacteria Affinity of ICG02-UBI₂₉₋₄₁. To investigate the bacteria-targeting ability of the ligand, UBI₂₉₋₄₁ was labeled with the visible fluorescent dye Rhodamine B (RhB) for laser confocal fluorescence microscope (LCFM, Olympus FV1000, Japan) imaging. The labeling process was conducted using a similar method described for the synthesis of ICG02-UBI₂₉₋₄₁. In detail, RhB (4.8 mg) was reacted with EDC·HCl/NHS (feed ratio of RhB/EDC·HCl/NHS = 1:1.2:1.2) in H₂O (0.5 mL). After stirring in the dark for 4 h at room temperature, the solution was added dropwise into UBI₂₉₋₄₁ dissolved in sodium borate buffer. The mixture was stirred at room temperature overnight in the dark. The crude product was purified by filtration through Sephadex G-15.

The dilution of the bacteria (1:10) was washed with saline and then resuspended in 500 μL of saline. Freshly prepared RhB-UBI₂₉₋₄₁ was resuspended in a small volume of sterile water and then added into the bacteria suspension. The bacteria suspension was placed in an incubated shaker for ~1 h at 37 °C. The suspension was centrifuged at 3000 rpm for 5 min to remove the redundant probes. The bacteria were washed three times with PBS before conducting LCFM scanning. Three independent LCFM assays were performed for each sample. The human normal cell (HBL-100) was also incubated with RhB-UBI₂₉₋₄₁ for 1 h following the method mentioned above. Subsequently, the cells were washed three times with PBS before LCFM imaging.

2.7. Dynamic Biodistribution of ICG02-UBI₂₉₋₄₁ in Normal Mice. Athymic nude mice and normal (Kunming) mice were purchased from Charles River Laboratories (Shanghai, China). All animal experiments were performed in compliance with the Animal Management Rules of the Ministry of Health of the People's Republic of China (documentation No. 55, 2001) and the guidelines for the Care and Use of Laboratory Animals of China Pharmaceutical University.

To investigate the dynamics of ICG02-UBI₂₉₋₄₁ ($n = 5$) in normal mice,²⁶ ICG02-UBI₂₉₋₄₁ (0.2 mL, 2 nmol) and ICG02 (as control) were injected respectively into the healthy ICR mice ($n = 5$) via tail vein and then the mice were monitored by NIR fluorescence imaging system over 48 h. The background images were taken for each mouse prior to the injection. The NIR fluorescent images were acquired at scheduled time points (1, 4, 6, 12, 24, and 48 h). To confirm the *in vivo* observations, the mice were sacrificed at predetermined time intervals (1, 2, 4, 6, 12, 24, and 48 h). Different organs (heart, liver, spleen, kidney, and intestine) were separated and washed with saline and then assembled for *ex vivo* fluorescence imaging.

2.8. Targeting Ability of ICG02-UBI₂₉₋₄₁ in Bacteria Infected Mice. To investigate the bacteria-targeting capability of the probe at the animal level, the mice were divided randomly into four groups ($n = 5$ per group, 20–22 mg), and the animal models of bacterial infection and sterile inflammation were built. The suspensions of *S. aureus*,²⁶ *E. coli*, or *P. aeruginosa* (10^5 CFU in 100 μL of saline) were subcutaneously

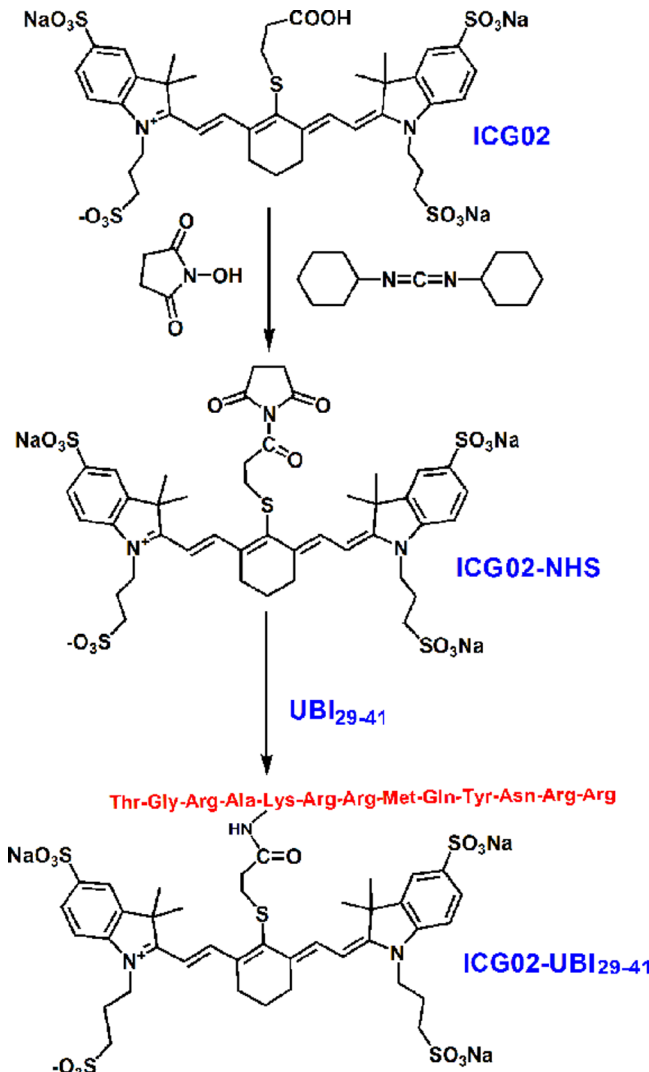


Figure 1. Synthetic schemes and structure of ICG02-UBI₂₉₋₄₁.

injected into the right axillary fossa of the mice, and LPS (1.0 mg/kg) was injected into the left axillary fossa. In order to compare the targeting capability of ICG02-UBI₂₉₋₄₁ in different bacteria, the mouse models simultaneously bearing *S. aureus* and *E. coli* were also built. The biodistribution of ICG02 (200 μL , 2 nmol) was also investigated as control. ICG02-UBI₂₉₋₄₁ (200 μL , 2 nmol) was intravenously injected into the subjected mouse at 24 h after inoculation and monitored for 48 h. The NIR fluorescent images were collected at 1, 4, 6, 12, 24, and 48 h, respectively, according to the method mentioned in section 2.7.

For blocking experiment, *S. aureus* or *E. coli* infected mice ($n = 5$ for each group) were injected with 200 μL of UBI₂₉₋₄₁ (2 nmol) first. Two hours later, the mouse models were injected with ICG02-UBI₂₉₋₄₁ (200 μL , 2 nmol). Then the mice were monitored by NIR fluorescence imaging system within 48 h postinjection of the probe.

2.9. Determination of the Minimum Inhibition Concentration. The minimum inhibitory concentrations (MIC) of CAP and CAP-UBI₂₉₋₄₁ were compared respectively by the broth microdilution method in accordance with the National Committee for Clinical Laboratory Standards method (NCCLS). *S. aureus* and *E. coli* were obtained from ATCC. Briefly, bacteria cultured for 12 h were inoculated into 5 mL of

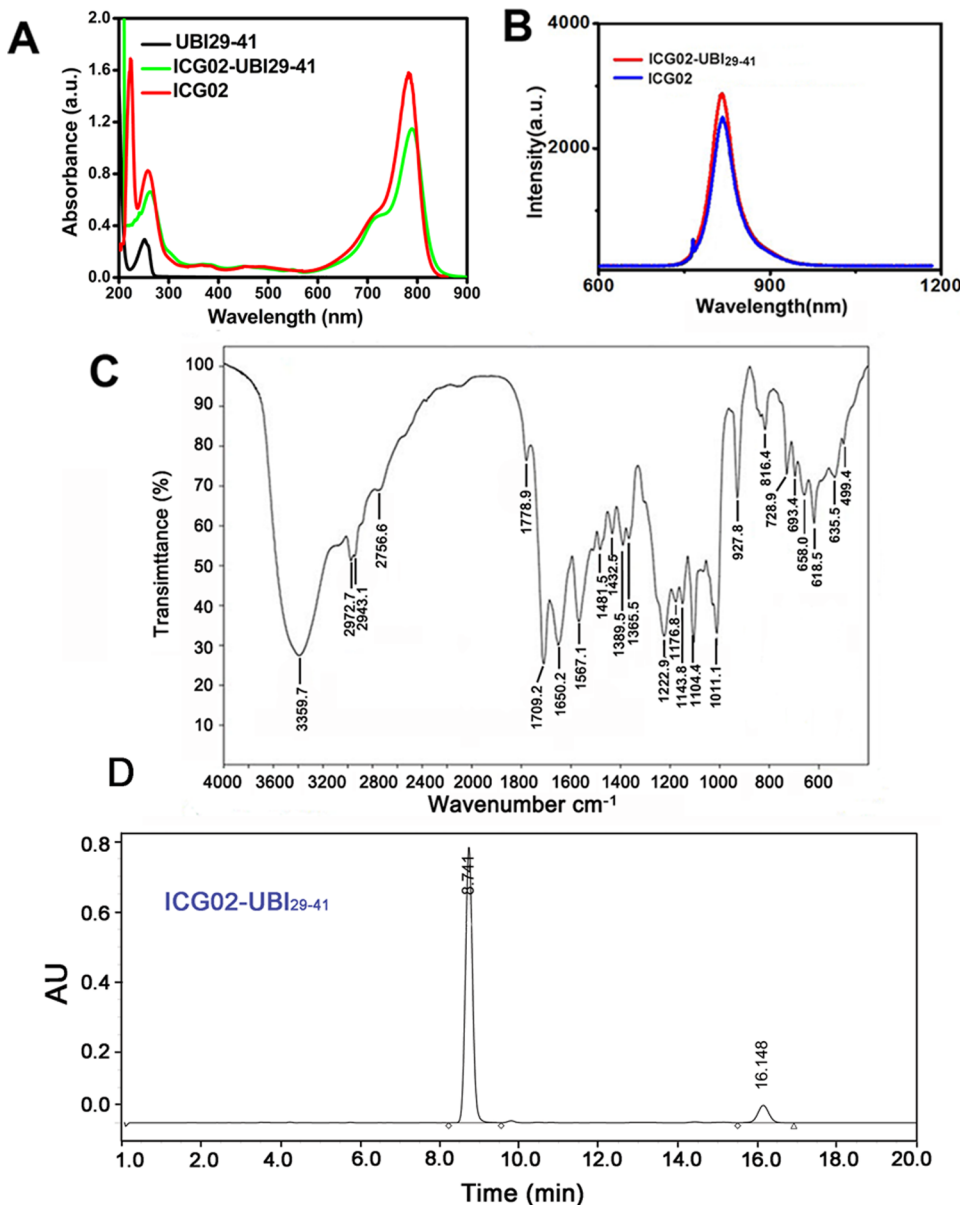


Figure 2. Characterization of ICG02-UBI₂₉₋₄₁. (A) Absorption spectra of UBI₂₉₋₄₁, the synthesized ICG02-UBI₂₉₋₄₁, and ICG02. (B) The emission spectra of ICG02-UBI₂₉₋₄₁ and ICG02. (C) FT-IR spectrum and (D) HPLC analysis of ICG02-UBI₂₉₋₄₁.

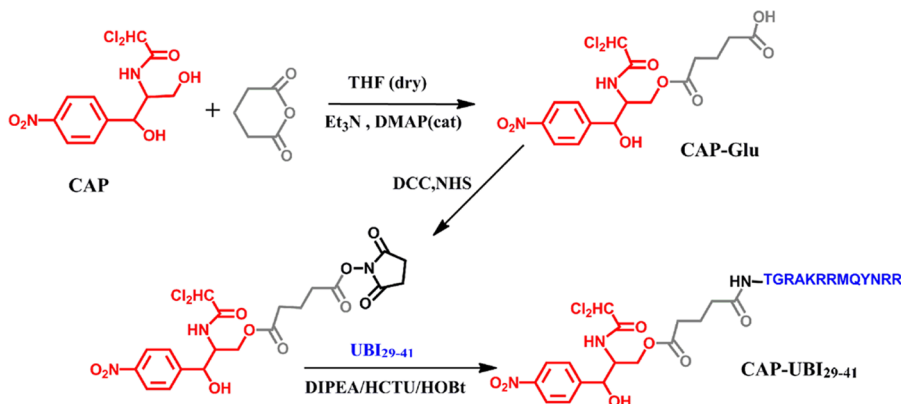


Figure 3. Synthesis and structure of CAP-UBI₂₉₋₄₁.

Mueller–Hinton broth and were allowed to enter log phase ($OD_{600} = 0.3$) after incubation for 2 h. A standard of this

bacteria suspension (100 μ L) was added to each well. Drugs were serially diluted from 500 to 0.5 μ g/mL in deionized water

(100 μ L) and added into the bacteria. The plates were incubated overnight at 37 °C. The optical densities of the microorganism solutions at 600 nm were measured as a function of time. The MIC was taken at the lowest concentration at which no visible growth was observed by the unaided eye (indicated by lack of visible turbidity). Broth containing bacteria without drug incubation was used as control, and the tests were repeated 5 times.

2.10. In Vitro Release of CAP from CAP-UBI_{29–41}. A calibration curve of CAP was established and used to estimate the amount of CAP contained in the conjugate and *in vitro* release profile of CAP from the conjugate. CAP-UBI_{29–41} (100 μ M) was incubated in PBS containing 25% of rat serum, serum free cell media, or PBS at 37 °C with stirring. Aliquots (100 μ L) were taken from the reaction solution at predetermined time intervals (starting from 30 min to 48 h). The free CAP was then extracted by 1.5 mL of ethyl acetate and was analyzed by RP-HPLC (detection wavelength: 270 nm). The mobile phase was acetonitrile/water (20:80) with a flow rate of 1.0 mL/min. The area under the curve was used to calculate the percentage of the released CAP.

2.11. In Vivo Study. **2.11.1. In Vivo Antibacterial Effects of CAP-UBI_{29–41}.** The neutropenic mouse thigh model with *S. aureus* infection was established following Boylan's report.²⁸ The mice were injected with cyclophosphamide intraperitoneally at day 1 (100 mg/kg) and day 4 (150 mg/kg), respectively. The mice infected with *S. aureus* were obtained by injection of a bacteria suspension (0.1 mL, 10⁷ CFU/mL) into the thigh muscles of anesthetized mice. Then the infected mice were randomly assigned into three groups: saline group, CAP group, and CAP-UBI_{29–41} group. Each of the group was treated with the sample every 2 days over 2 weeks as described below: free CAP and CAP-UBI_{29–41} were administrated into different groups of mice at a dose of 5 mg CAP/kg every 2 days. The healthy mice were injected with saline as the control group. The treatment effect was assessed by measuring the circumference of the thigh and the body weight. Six mice of every group were sacrificed at 5 days postinjection. Thigh muscles were removed for histopathology evaluation, and tissue was homogenized for bacteria counts. The number of colony-forming units (CFU) was counted, and the data was expressed as mean values \pm standard deviation ($n = 6$).

2.11.2. Acute Toxicity Test in Mice. The acute toxicity of CAP-UBI_{29–41} was investigated in the normal mice. Briefly, 30 ICR mice were divided randomly into three groups, including the saline group, CAP group, and CAP-UBI_{29–41} group. Free CAP (100 mg) and CAP-UBI_{29–41} (100 mg CAP) were injected via tail vein into the mice. Blood samples were drawn from the eye socket to prepare the serum samples and whole blood at 7 days postinjection. The serum biochemical parameters including alanine aminotransferase (ALT), aspartate aminotransferase (AST), creatinine kinase (CK), blood urea nitrogen (BUN), and creatinine (Cr) indexes of the blood samples were all examined. The leukocyte and neutrophils of the whole blood samples were also measured.

2.12. Statistics. Significant differences were determined using the Student's *t* test where differences were considered significant ($p < 0.05$). All of the data are presented as mean \pm standard deviation (SD).

3. RESULTS

3.1. Synthesis and Optical Characterization of ICG02-UBI_{29–41} and CAP-UBI_{29–41}.

The synthesis procedure of

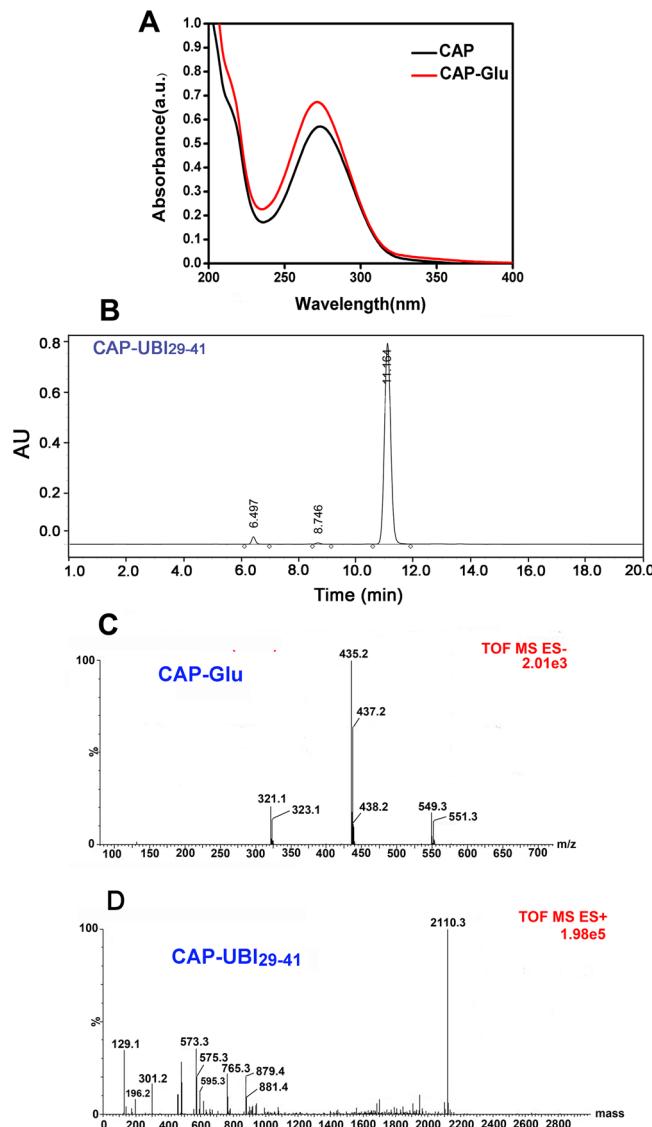


Figure 4. Characterization of CAP-Glu and CAP-UBI_{29–41}. (A) Absorption spectra of the synthesized intermediate product CAP-Glu and CAP. (B) HPLC analysis of CAP-UBI_{29–41}. (C) Q-TOF MS profile of CAPGlu ([M⁺] 437.2). (D) Q-TOF MS profile of CAP-UBI_{29–41} ([M⁺] 2110.3).

ICG02-UBI_{29–41} is illustrated in Figure 1.²⁶ The absorption spectra of ICG02-UBI_{29–41}, ICG02, and UBI_{29–41} are demonstrated in Figure 2A. The characteristic absorption peaks of ICG02 (780 nm) were observed in the absorption spectrum of ICG02-UBI_{29–41}. The characteristic fluorescence peak of ICG02-UBI_{29–41} was similar to that of the free dye ICG02 (810 nm), as shown in Figure 2B. These results demonstrate that the conjugation of UBI_{29–41} to ICG02 did not influence the optical properties of the dye. FT-IR measurements were further performed to characterize the molecular structure of ICG02-UBI_{29–41}, as shown in Figure 2C. The characteristic peaks at 3389.7 cm⁻¹ (ν_{NH} , s), 1650.6 cm⁻¹ ($\nu_{\text{C=O}}$, s), and 1567.1 cm⁻¹ (β_{NH} , s) all correspond to the amide bond of ICG02-UBI_{29–41}. Figure 2D shows the purity analysis of ICG02-UBI_{29–41} by HPLC.

CAP-UBI_{29–41} was synthesized following the procedure shown in Figure 3. The successful preparation of the intermediate product (CAP-Glu) was first confirmed by UV-vis absorption

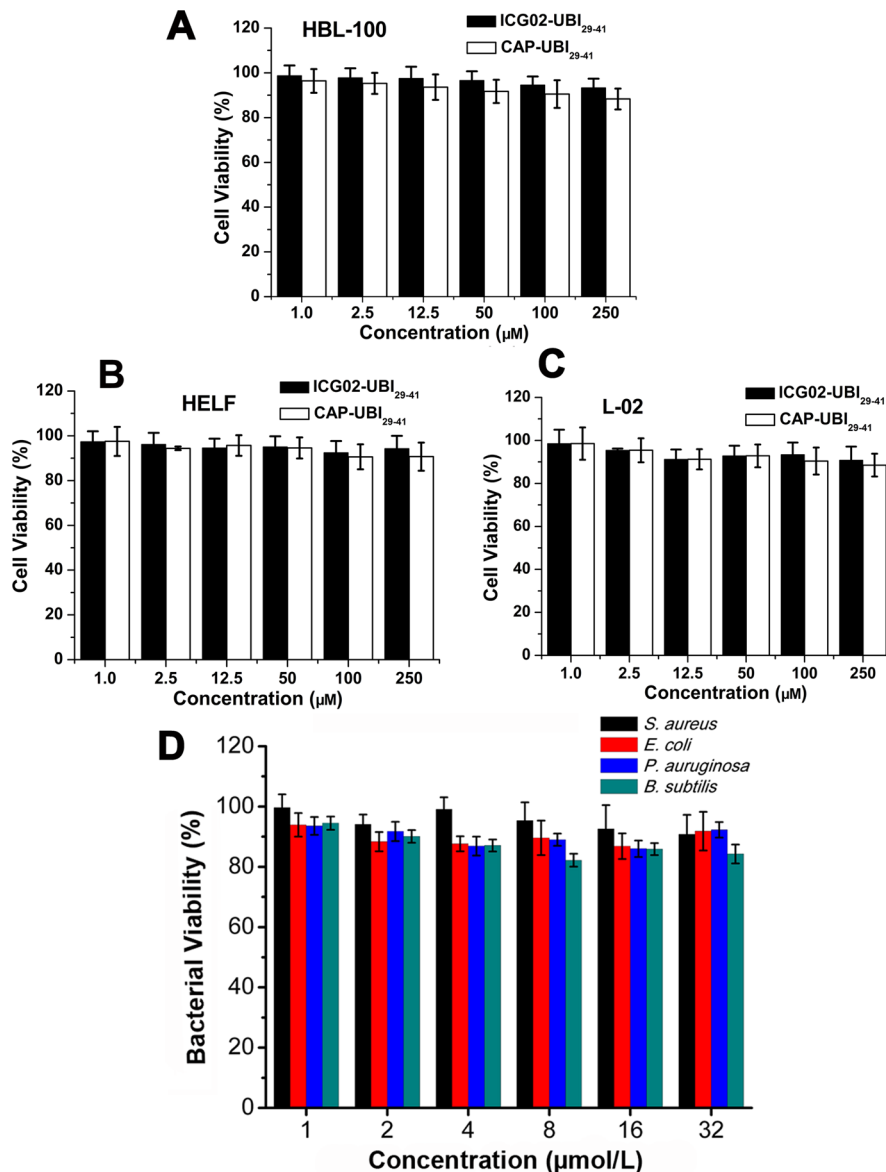


Figure 5. Cytotoxicity evaluation of ICG02-UBI₂₉₋₄₁ and CAP-UBI₂₉₋₄₁. The cell viability of three normal cell lines (A) HBL-100, (B) HELF, and (C) L-02 after incubation with ICG02-UBI₂₉₋₄₁ was investigated. (D) The antibacterial activity of ICG02-UBI₂₉₋₄₁ on four bacteria (*S. aureus*, *E. coli*, *P. aeruginosa*, and *B. subtilis*) was examined by broth microdilution.

spectroscopy and electrospray mass spectrometry (EI-MS). As shown in Figure 4A, CAP-Glu has an absorption peak (270 nm) corresponding to the characteristic absorption peak of CAP. The content of CAP-UBI₂₉₋₄₁ after purification was analyzed by HPLC (Figure 4B). MS spectra of CAP-Glu and CAP-UBI₂₉₋₄₁ are shown in Figure 4C,D, respectively.

3.2. In Vitro Cytotoxicity, Antibacterial Activity, and Bacteria Affinity. The cytotoxicity of ICG02-UBI₂₉₋₄₁ and CPA-UBI₂₉₋₄₁ on three normal human cell lines (L02, HBL-100, and HELF) was measured (Figure 5A–C). The results showed that even at the highest concentration (250 μM) the cell viabilities were above 90% for ICG02-UBI₂₉₋₄₁ and above 85% for CAP-UBI₂₉₋₄₁. This result suggests that both ICG02-UBI₂₉₋₄₁ and CPA-UBI₂₉₋₄₁ have very low cytotoxicity on human cells. In addition, the *in vitro* antibacterial activity of ICG02-UBI₂₉₋₄₁ was investigated (Figure 5D). For the four bacteria strains, ICG02-UBI₂₉₋₄₁ showed a very low inhibition ratio. The survival rate of the bacteria was over 90% in a wide

concentration range (1.0–32 $\mu\text{mol/L}$). These results suggest that ICG02-UBI₂₉₋₄₁ has no antibacterial ability, and this property is beneficial to further biomedical applications.

As shown in Figure 6A, red fluorescence could be observed at the bacterial cell wall after incubation with RhB-UBI₂₉₋₄₁. However, no fluorescence appeared in the normal human cell (HBL-100). These results demonstrate that UBI₂₉₋₄₁ selectively binds to bacteria. The zeta potentials of *S. aureus* and *E. coli* are shown in Figure 6B. The zeta potentials of *E. coli* ($-10 \text{ mV} \sim -15 \text{ mV}$) and *S. aureus* ($-17 \text{ mV} \sim -23 \text{ mV}$) validated that these bacteria possessed anionic charge on their cell membrane.

3.3. Dynamic Biodistribution and Targeting Ability of ICG02-UBI₂₉₋₄₁ in Mice. To better understand the physiological behavior of the probe, the dynamics of ICG02-UBI₂₉₋₄₁ was investigated in healthy ICR mice ($n = 5$). ICG02 was utilized as control. As shown in Figure 7A, ICG02-UBI₂₉₋₄₁ was cleared from the mice quickly (within 24 h). Figure 7B demonstrates that the fluorescence signals of ICG02 initially

spread throughout the whole body by 1 h postinjection and gradually accumulated in the bladder. At about 48 h postinjection, the fluorescence signal nearly disappeared except for the residual signal in the bladder. Figure 7C displayed the distribution of ICG02-UBI_{29–41} in the main organs at 1, 2, 4, 6, 12, and 24 h ($n = 5$), which coincides with the result from *in vivo* observations. Consistently, the probe was first dispersed in all the organs and gradually accumulated in the kidney and bladder. At 24 h, the probe was almost cleared from the subjected mice.

To assess the bacteria-targeting capability of the probe and its ability to discriminate between bacterial infection and sterile inflammation, the biodistribution of the probes in different mouse models were studied. The dynamic distribution of ICG02 in the same mouse models was also investigated, which was introduced as control. As shown in Figure 8A–C, there were no obvious fluorescence signals detected either in the sites of bacterial infection or sterile inflammation. The typical images of ICG02-UBI_{29–41} showed that the fluorescence signal was initially distributed all over the body at 1 h. The infection abscesses could be clearly distinguished from the surrounding tissue at 4 h and distinct fluorescence signals were easily detected until 24 h postinjection (Figure 8D–F). In contrast, nearly no fluorescence was observed from the sterile inflammation sites at 48 h postinjection. As shown in Figure 8G, the fluorescence signals in *S. aureus* infections could be observed until 24 h, whereas the fluorescence signals in *E. coli* infected sites disappeared at 24 h. The blocking experiment result shown in Figure 8H,I exhibited the receptor specificities of ICG02-UBI_{29–41}. There is no obvious fluorescence signal at the bacteria (*S. aureus* and *E. coli*) infection sites within 48 h postinjection. Free UBI_{29–41} successfully reduced the accumulation of the probe in bacteria (*S. aureus* and *E. coli*) infected sites. The contrast ratio of abscess to normal tissue (A/N) was semiquantified by ROI analysis of the fluorescence images, as shown in Figure 8J. The results indicate that the A/N ratio reached the maximum (4.9 for *S. aureus*; 3.6 for *E. coli*) at 4 h postinjection.

3.4. Minimum Inhibition Concentration and Stability of CAP-UBI_{29–41}. The MICs of CAP-UBI_{29–41} and CAP against *E. coli* and *S. aureus* were investigated in the wide incubation concentration range of 0.5 to 256 $\mu\text{g}/\text{mL}$ (as shown in Table 1). The growth of the bacteria was effectively inhibited by both CAP-UBI_{29–41} and CAP. The MICs of CAP-UBI_{29–41} against *S. aureus* and *E. coli* were 15.0 ± 2.6 and $3.8 \pm 0.9 \mu\text{mol}/\text{L}$, respectively. The MICs of the CAP against *S. aureus* and *E. coli* were 24.8 ± 5.7 and $6.2 \pm 1.7 \mu\text{mol}/\text{L}$, respectively.

The standard curve of CAP was built by absorbance measurements as shown in Figure 9A. The release profiles of CAP from CAP-UBI_{29–41} in different medium (PBS, cell culture and rat plasma) are displayed in Figure 9B. CAP-UBI_{29–41} displayed faster release of CAP in cell culture medium (38% at 4 h), intermediate release in rat plasma (27.4% at 4 h), and lower release in PBS buffer (18.9% at 4 h).

3.5. Antibacterial Effects of CAP-UBI_{29–41} on Infected Mice. The *in vivo* antibacterial effects of CAP-UBI_{29–41} were evaluated in *S. aureus*-infected mouse models. The changes of the leg abscess are shown in Figure 10A. Figure 10B shows the body weight changes of different groups (saline, CAP, and CAP-UBI_{29–41}), respectively. The decrease of body weight for the saline group was up to 32.8% of the original weight, indicating the severity of bacterial infection. In contrast, the body weight of the CAP-UBI_{29–41} group decreased marginally,

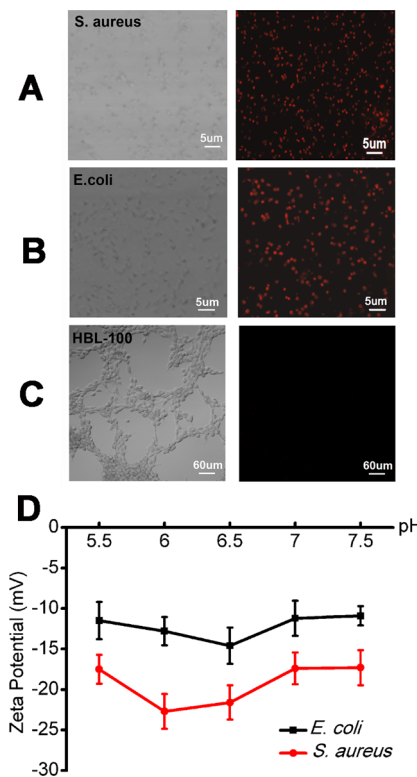


Figure 6. Laser confocal microscopy images of (A) *S. aureus*, (B) *E. coli*, and (C) human normal cell HBL-100 after incubation with RhB-UBI_{29–41} for 1 h. (D) The zeta potentials of the bacteria (*E. coli* and *S. aureus*) at different pH values (5.5–7.5).

and the body weight loss of the CAP group was 20.3% of the original weight. The abscess size changes are shown in Figure 10C. For the saline-treated group, the thigh circumference was 20 mm, which is 2-fold of the normal size, and additionally, the leg muscles became ulcerated, thus increasing the severity of the infection. In contrast, the thigh circumference for the CAP-UBI_{29–41}-treated group became smaller and the thigh maintained a normal size of 10 mm on day 7. A slower healing process was observed in the free CAP-treated group. This result demonstrates that CAP-UBI_{29–41} has a better antibacterial effect than free CAP.

The tissue homogenate bacteria colony count is shown in Figure 10D. The thigh muscles were removed after 4 days of treatment to quantify the CFU of *S. aureus*. As shown in Figure 10D, the CFU was $6 \times 10^{10}/\text{g}$ for the CAP-treated group. However, the CFU for the CAP-UBI_{29–41}-treated group was $2 \times 10^{10}/\text{g}$. These results further demonstrate that CAP-UBI_{29–41} possesses a better antibacterial effect than CAP. Neutrophils are the primary white blood cells that respond to bacterial infection. As shown in Figure 10E, CAP-UBI_{29–41} treatment largely reduced the percentage of neutrophils in the thigh muscles in comparison with the group injected with saline and CAP. These findings indicate that CAP-UBI_{29–41} could effectively suppress bacterial infection.

3.6. Acute Toxicity. The acute toxicity of CAP-UBI_{29–41} was assessed in healthy mice. To evaluate its toxicity on the liver, heart, and kidney, ALT, AST, CK, BUN, and Cr of mice serum samples were determined at 4 days postinjection. As listed in Table 2, the treatment with CAP and CAP-UBI_{29–41} did not improve the levels of these parameters in comparison with the control group, implying that CAP-UBI_{29–41} and CAP

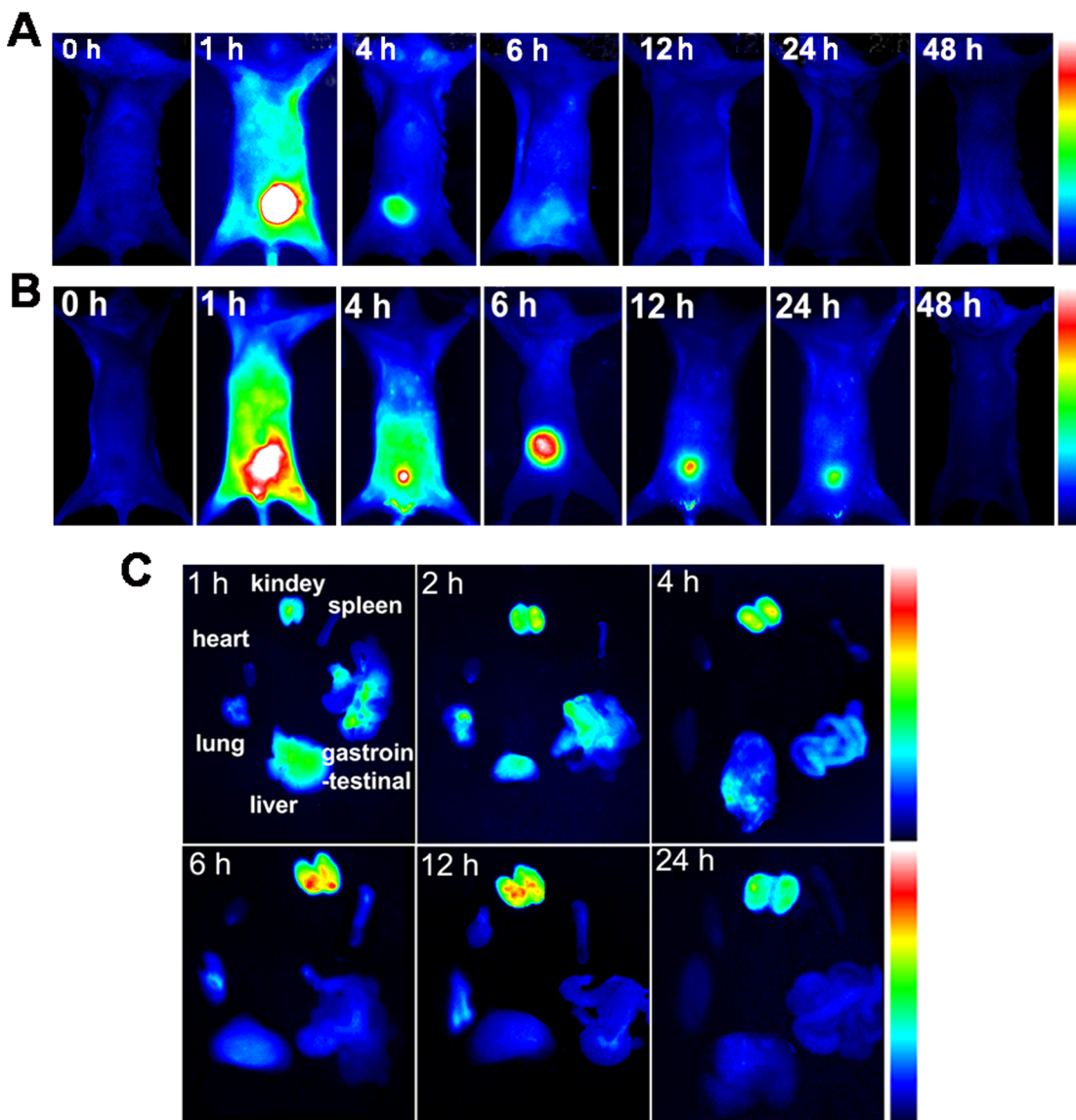


Figure 7. Biodistribution of (A) ICG02- UBI_{29-41} and (B) ICG02 in healthy ICR mice within 48 h, which was monitored by NIR fluorescence imaging system. (C) The main organs excised from the mice at the determined time points (1, 2, 4, 6, 12, and 24 h).

did not cause significant damage to liver, heart, and kidney functions at the injected dose level.

Since the extremely high doses of CAP induce a decrease in neutrophil levels, the leukocyte and neutrophils of whole blood samples from CAP- UBI_{29-41} -treated mice were also measured to assess the acute toxicity. As listed in Table 3, the free CAP caused a significant decrease in neutrophil count ($0.24 \times 10^9/\text{L}$) compared to the control group ($1.46 \times 10^9/\text{L}$). In contrast, the effect of CAP- UBI_{29-41} was not apparent ($0.78 \times 10^9/\text{L}$), further indicating the lower toxicity of CAP- UBI_{29-41} in mice.

4. DISCUSSION

Current challenges presented by bacterial infection including the side effects of antibiotic therapy, the increasing spread of multidrug resistance, the negative consequences of clearing the commensal bacterial flora, and difficulties in developing prophylactic vaccines continue to fuel significant concerns, particularly in healthcare settings. This study investigated the potential of human antimicrobial peptide fragment UBI_{29-41} to contribute to the targeting therapy of bacterial infections. CAP

is considered a prototypical broad-spectrum antibiotic, and it is frequently the first choice for treatment of bacterial meningitis and brain abscesses. However, in some countries, CAP has been excluded from antibacterial agents because of its side effects to neutrophils. In this study, CAP- UBI_{29-41} was successfully synthesized and systematically characterized. The peptide UBI_{29-41} was used as a targeting ligand to increase the accumulation of CAP- UBI_{29-41} in the bacterial infection sites. To visualize the distribution of UBI_{29-41} *in vivo*, NIR fluorescent dye ICG02 was covalently attached to UBI_{29-41} , and this successful conjugation of ICG02- UBI_{29-41} was confirmed by the optical spectra (Figure 2A,B), MS, and ^1H NMR. The targeting capability of the antimicrobial peptide fragment UBI_{29-41} was validated both at the bacteria level and animal level via conjugation with fluorescent dye (RhB or ICG02). The probe exhibited higher accumulation in *S. aureus* infections than in *E. coli* infections (Figure 8G). This could be attributed to the higher negative charge of *S. aureus*, which would allow the probe to have a better targeting capability toward *S. aureus* than *E. coli*. These results are consistent with the zeta potential of *S. aureus* and

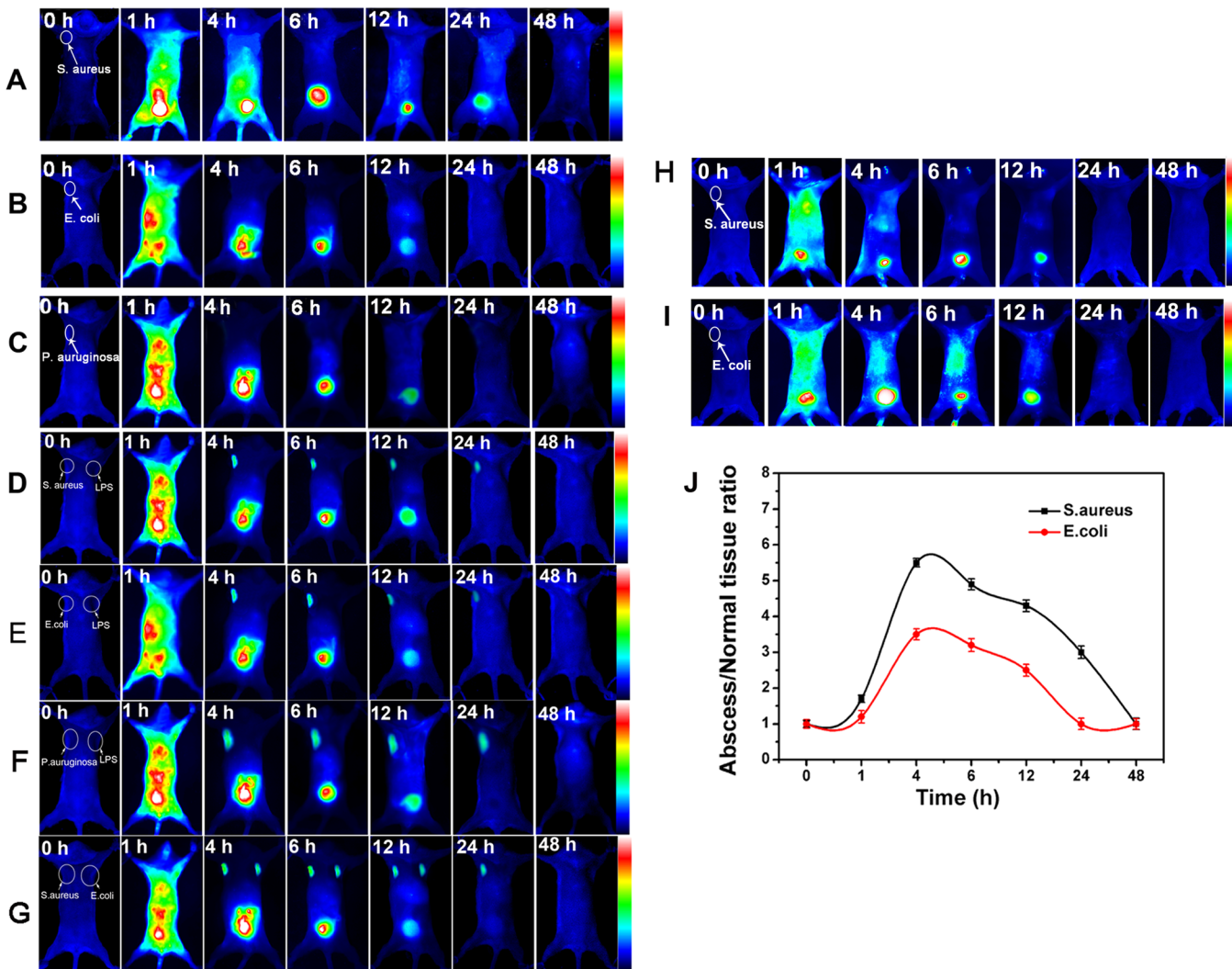


Figure 8. NIR fluorescence images of ICG02 and ICG02-UBI₂₉₋₄₁ after injecting into different mouse models. The biodistribution of ICG02 in ICR mice infected (A) with *S. aureus* (right) and LPS (left); (B) with *E. coli* (right) and LPS (left); (C) with *P. aeruginosa* (right) and LPS (left). The biodistribution of ICG02-UBI₂₉₋₄₁ in ICR mice infected (D) with *S. aureus* (right) and LPS (left); (E) with *E. coli* (right) and LPS (left); (F) with *P. aeruginosa* (right) and LPS (left); (G) *S. aureus* (right) and *E. coli* (left). The *in vivo* UBI₂₉₋₄₁ blocking experiment was performed in (H) *S. aureus* and (I) *E. coli* mice models by injection of UBI₂₉₋₄₁ first before ICG02-UBI₂₉₋₄₁ injection. (J) The abscess/normal tissue ratios of ICG02-UBI₂₉₋₄₁ at different time points in *S. aureus* and *E. coli* infected mouse model.

E. coli in Figure 6. Additionally, the different accumulation of ICG02-UBI₂₉₋₄₁ in *S. aureus* and *E. coli* could also be attributed to the different cell wall structure of these two bacteria. *S. aureus* is a Gram-positive bacterium and is characterized by thick cell walls containing rich peptidoglyca. *E. coli* is a Gram-negative bacterium with thin cell walls and low peptidoglyca content. Therefore, these two kinds of bacteria demonstrate different affinities toward ICG02-UBI₂₉₋₄₁.

In our previous studies, we have shown the great potential of NIR fluorescence imaging in applications ranging from cancer detection to image-guided surgery.^{29–31} Several studies have so far been published on the highly promising methods for early detection of bacterial infections with fluorescent agents. Ning et al.³² used a maltodextrin-IR786 conjugate to detect three bacteria (*E. coli*, *S. aureus*, *P. aeruginosa*, and *Bacillus subtilis*) with strong bacteria-specific signals in rats after intravenous administration (TBR ratios of 26). However, this probe tends to accumulate only in metabolically active bacteria. Van Oosten et al.³³ explored the use of fluorescently labeled vancomycin (vanco-800CW) to specifically target and detect infections

Table 1. Determination of Minimum Inhibitory Concentrations of CAP-UBI₂₉₋₄₁

strains	CAP-UBI ₂₉₋₄₁ ($\mu\text{mol/L}$)	CAP ($\mu\text{mol/L}$)	significance
<i>E. coli</i>	3.8 ± 0.9	6.2 ± 1.7	$*(p < 0.05)$
<i>S. aureus</i>	15.0 ± 2.6	24.8 ± 5.7	$*(p < 0.05)$

caused by Gram-positive bacteria. Kong et al.³⁴ demonstrated the *in vivo* detection of *Mycobacterium tuberculosis* with an activatable probe consisting of a β -lactam moiety linking a fluorophore to a fluorescence quencher. The β -lactam ring could be cleaved by β -lactamase. However, not all bacteria produce β -lactamase, and thus, this probe is limited in its further clinical applications.

To validate that UBI₂₉₋₄₁ could target to the bacteria-infected tissues at the early stage, the bacteria-infected mouse models were built by injecting the suspensions of *S. aureus*, *E. coli*, or *P. aeruginosa* (10^5 CFU in $100 \mu\text{L}$ of saline) subcutaneously into the right axillary fossa of the mice and the mice were used for imaging after 24 h inoculation. Our group's previous work

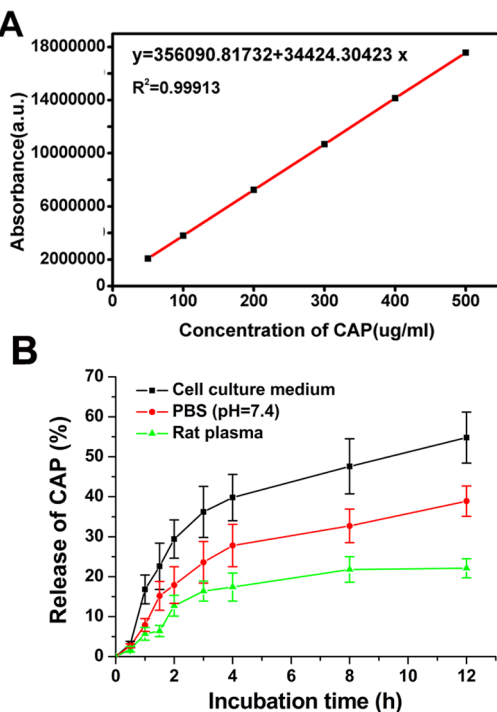


Figure 9. Stability of CAP-UBI_{29–41} in three solutions. (A) The regression equation of CAP and the related standard curve: Y(OD) = 356090.81732 + 34424.30423X ($R^2 = 0.99913$). The linear range of the standard curve was from 0.5–500 $\mu\text{g}/\text{mL}$. The stand curve was evaluated by HPLC (CH_3OH). (B) The release profile of CAP from CAP-UBI_{29–41} in different incubation medium (cell culture medium, PBS, and rats plasma) at 37 °C. The incubation time continued until 12 h.

validated that the probe sensitivity is correlated with both the bacteria number and the incubation time.³⁵ The probe's sensitivity improves accordingly as the bacteria number and incubation time increase, which provides references for the design of the bacteria imaging probes. Here, ICG02-UBI_{29–41} enables specific detection of bacteria with high sensitivity and accuracy. As expected, *in vitro* and *in vivo* evaluations showed highly specific binding of ICG02-UBI_{29–41} to the bacteria (*S. aureus*, *E. coli*, or *P. aeruginosa*). In terms of biodistribution, strong fluorescence signals were detected in the kidney and urine, while a minimal signal was detected in the liver. Importantly, the signals emitted from bacteria-infected tissues could be clearly distinguished from the kidney, bladder, and liver signals. No significant fluorescent signals were detected in other organs. Notably, we were able to discriminate between bacterial infection and sterile inflammation. UBI_{29–41} (MW 1.69 kDa) is a cationic human antimicrobial peptide fragment with the amino acid sequence Thr-Gly-Arg-Ala-Lys-Arg-Arg-Met-Gln-Tyr-Asn-Arg-Arg (TGRAKRRMQYNRR), thus with six positively charged residues (5 Arg + 1 Lys).³⁶ The membranes of bacteria are coated with negatively charged lipoteichoic acid and phospholipids, while the negatively charged lipids face the cytoplasm for normal or malignant cells. The basis of the bacteria-specific activity of UBI_{29–41} bound conjugates stems from the interaction between the peptide's cationic (positively charged) domains with the surface (negatively charged) of the bacteria. Therefore, ICG02-UBI_{29–41} could be utilized to detect the vast majority of clinically relevant bacterial infections *in vivo* and CPA-UBI_{29–41} could be applied for bacteria-targeting therapy, making them more attractive for biomedical applications.

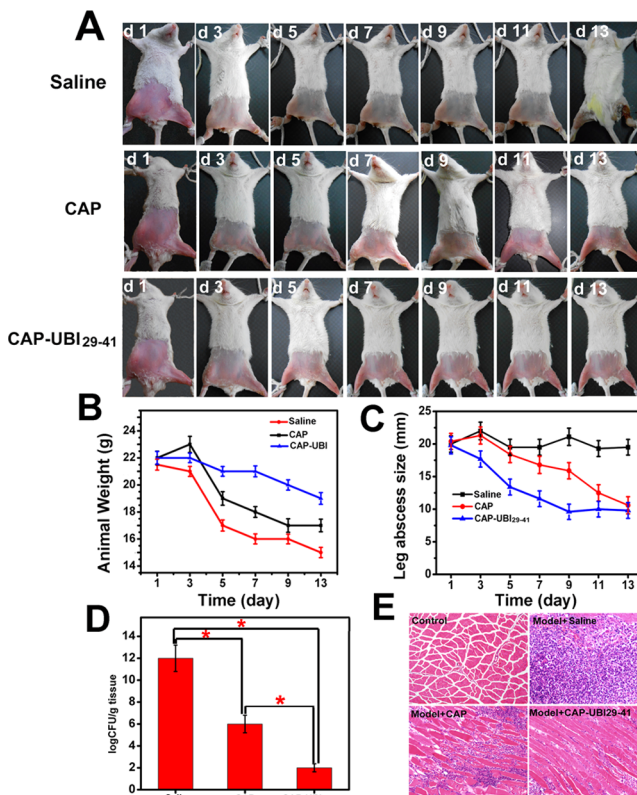


Figure 10. *In vivo* antibacterial effect against *S. aureus* infected ICR mice. (A) The photograph of the leg abscess in different groups (saline, CAP, and CAP-UBI_{29–41}) within 13 days postinjection of CAP-UBI_{29–41}. (B) Animal weights and (C) the leg circumference changes of ICR mice infected with *S. aureus* as a function of therapy time (day 1 to day 13). (D) CFU of *S. aureus* for different drug treated groups (saline, CAP, and CAP-UBI_{29–41}) at the fourth day of treatment. (E) Tissue sections of thigh muscles excised from the different groups (normal mice, saline, CAP, and CAP-UBI_{29–41}) at the fourth day of treatment. For hematoxylin and eosin staining, the inflammation cells were stained bluish violet (image magnification is 200 \times). Data were given as mean ($n = 6$) \pm SD.

Table 2. Serological Analysis of the Mice Injected with NaCl, CAP, and CAP-UBI_{29–41}

Groups	ALT (IU/L)	AST (IU/L)	BUN (mmol/L)	Cr ($\mu\text{mol}/\text{L}$)	CK (IU/L)
NaCl	62 \pm 4	76 \pm 7	6.6 \pm 1.2	57.7 \pm 5.5	283 \pm 13
CAP	64 \pm 5	80 \pm 5	6.9 \pm 1.8	58.0 \pm 6.2	290 \pm 20
CAP-UBI _{29–41}	61 \pm 2	79 \pm 4	6.4 \pm 1.0	57.4 \pm 5.0	287 \pm 16

Table 3. Quantitative Counts of Neutrophils in the Whole Blood of the Mice Injected with NaCl, CAP, and CAP-UBI_{29–41}

different groups	leukocytes ($\times 10^9/\text{L}$)	neutrophils ($\times 10^9/\text{L}$)
saline	8.17	1.46 (17.9%)
CAP-UBI _{29–41}	7.3	0.98 (13.4%)
CAP	4.46	0.24 (5.3%)

than vanco-800CW or β -lactamase-specific smart activatable probes.

Hydrolases are a class of enzymes that primarily exist in cells that catalyze the hydrolysis of a chemical bond and play an important role in metabolism.³⁷ CAP was covalently attached

to UBI_{29–41} with a linker (glutaric anhydride). The ester bond between CPA and glutaric anhydride is easy to break down with hydrolase catalysis. Therefore, the release profile of CAP from CAP-UBI_{29–41} was dependent on the medium (cell culture medium, rat plasma, and PBS). Obviously, the release rate of CAP from CAP-UBI_{29–41} in cell culture medium and rat plasma was faster than that in cell-free environment, which could be attributed to hydrolase catalysis. The releasing ratios of CAP from CAP-UBI_{29–41} are less than 50% within 8 h, which ensures that most of the drug could reach the bacteria-infected tissue before being hydrolyzed by hydrolase. Therefore, CAP-UBI_{29–41} could serve as a pro-drug with a targeting moiety for bacteria delivery. CAP is an antibiotic which is useful for the treatment of a number of bacterial infections. It is more effective against a wide variety of Gram-negative bacteria than Gram-positive bacteria. Therefore, the MIC of CAP observed for Gram negative *E. coli* was lower than for Gram positive *S. aureus* (Table 1). Although a higher accumulation of ICG02-UBI_{29–41} was observed in *S. aureus*, the MIC of CAP-UBI_{29–41} was still higher for *S. aureus* ($15.0 \pm 2.6 \mu\text{mol/L}$) than *E. coli* ($3.8 \pm 0.9 \mu\text{mol/L}$). This result validated that UBI_{29–41} acting as a bacteria-targeting ligand could improve the accumulation of CAP at bacteria-infected sites but could not change the therapeutic efficacy of CAP between Gram-negative bacteria and Gram-positive bacteria.

Treatment of the bacteria-infected tissue during its early stages is most effective and significant. Currently, a variety of approaches are being evaluated including small molecular antibiotics,³⁸ bacteriophages,³⁹ antimicrobial peptide,⁴⁰ and antivirulence or drug potentiators.⁴¹ Here, we focused on bacteria-targeting therapy. The advantages of targeting include improved drug efficacy, reduced side effects, and reduced clearance of mutualist bacteria, which might influence a variety of diseases such as asthma, eczema, diabetes, and so on. The *in vivo* antibacterial study and the bacteria counting (Figure 10A,D) indicated that the antibacterial effect of CAP-UBI_{29–41} was significantly improved in comparison with CAP. The mice treated with CAP-UBI_{29–41} did not show significant decrease in body weight, whereas the group of mice treated with CAP exhibited significant weight loss. Most importantly, the acute toxicity experiments (Table 2) demonstrated that CAP-UBI_{29–41} had no toxicity on liver, heart, and kidney. In particular, it shows a lower toxicity on neutrophils than free CAP. These results demonstrate that CAP-UBI_{29–41} greatly reduced the toxicity of CAP and enhanced the antibacterial activity of the drug. Van Oosten et al.³³ demonstrated that a strong fluorescence signal emanated from the abscesses of bacteria-infected mice with an intravenous dose of 1 mg kg^{-1} vanco-800CW, which is 10-fold lower than the therapeutic dose in humans (10 mg kg^{-1}). However, the antibacterial effect of vancomycin after conjugation was not validated in their work. All the results in this work showed that CAP-UBI_{29–41} is a promising antibacterial agent that did not only enhance the antibacterial effect of CAP but also minimize its toxic side effects on normal cells/tissues. The strategy of conjugation of CAP with the bacteria-targeting peptide opens up a new avenue for design and synthesis of novel antibacterial agents as an alternative to antibiotics.

There is an acute need to develop new methods for treating bacterial infections. Improving targeting and delivery can reinvigorate old drugs or facilitate new drug development, especially in the case of toxic or poorly soluble drugs. Key to improved design is an intimate understanding of the delivery challenges. Improving the accumulation specificity at sites where pathogenic bacteria reside will overcome challenges like clearance

by the immune system, biotoxicity, and so on. It will be necessary to continue exploring molecular mechanism of drug resistance, microbial drug susceptibility, and biofilm formation to determine the optimal pathways that can be utilized for bacteria-targeting therapy.

5. CONCLUSION

In summary, ICG02-UBI_{29–41} and CAP-UBI_{29–41} conjugates were synthesized successfully. The targeting capability of the peptide UBI_{29–41} has been validated both at the bacterial and animal level. In comparison with the precursor (CAP), CAP-UBI_{29–41} exhibited several advantages including broad antibacterial activity and low cytotoxicity on normal cells and tissues. The disease-targeting delivery system of antibiotics may allow the reintroduction of drugs that have long been excluded from antibacterial use (because of toxicity and/or low selectivity). Reintroduction of such drugs into the antibacterial application may be useful for inhibiting emerging antibiotic-resistant bacteria. Hence, CAP-UBI_{29–41} is a promising antibacterial drug for bacteria-targeting therapy.

■ AUTHOR INFORMATION

Corresponding Author

*E-mail: guyueqing@hotmail.com. Tel: +86-25-83271080. Fax: +86-25-83271046.

Notes

The authors declare no competing financial interest.

■ ACKNOWLEDGMENTS

The authors are grateful to National Basic Research Program of China (973 Program Grant No: 2015CB755500) and Natural Science Foundation Committee of China (NSFC 61335007, 81220108012, 81371684, and 81328012) for their financial support.

■ REFERENCES

- (1) Lipsky, B. A.; Itani, K.; Norden, C. Treating foot infections in diabetic patients: a randomized, multicenter, open-label trial of linezolid versus ampicillin-sulbactam/ amoxicillin-clavulanate. *Clin. Infect. Dis.* **2004**, *38*, 17–24.
- (2) Reiber, G. E.; Pecoraro, R. E.; Koepsell, T. D. Risk factors for amputation in patients with diabetes mellitus: A case-control study. *Ann. Intern. Med.* **1992**, *117*, 97–105.
- (3) Signore, A.; D'Alessandria, C.; Lazzeri, E.; Dierckx, R. Can we produce an image of bacteria with radiopharmaceuticals? *Eur. J. Nucl. Med. Mol.* **2008**, *35*, 1051–1055.
- (4) Ning, X.; Lee, S.; Wang, Z.; Kim, D.; Stubblefield, B.; Gilbert, E.; Murthy, N. Maltodextrin-based imaging probes detect bacteria *in vivo* with high sensitivity and specificity. *Nat. Mater.* **2011**, *10*, 602–607.
- (5) Barton, R. C. Laboratory diagnosis of invasive aspergillosis: from diagnosis to prediction of outcome. *Scientifica* **2013**, *2013*, 459405–459423.
- (6) Ebenhan, T.; Zeevaart, J. R.; Venter, J. D.; Govender, T.; Kruger, G. H.; Jarvis, N. V.; Sathekge, M. M. Preclinical evaluation of 68Ga-labeled 1,4,7-triazacyclononane-1,4,7-triacetic acid-ubiquicidin as a radioligand for PET infection imaging. *J. Nucl. Med.* **2014**, *55*, 308–314.
- (7) Coleman, M. T.; Maiello, P.; Tomko, J.; Frye, L. J.; Fillmore, D.; Janssen, C.; Klein, E.; Lin, P. L. Early Changes by (18)-Fluorodeoxyglucose positron emission tomography coregistered with computed tomography predict outcome after *Mycobacterium tuberculosis* infection in cynomolgus macaques. *Infect. Immun.* **2014**, *82*, 2400–2404.

- (8) Herbst, T.; Van Deerlin, V. M.; Miller, W. T., Jr. The CT appearance of lower respiratory infection due to parainfluenza virus in adults. *AJR, Am. J. Roentgenol.* **2013**, *201*, 550–554.
- (9) Tang, E. N.; Nair, A.; Baker, D. W.; Hum, W.; Zhou, J. In vivo imaging of infection using a bacteria-targeting optical nanoprobe. *J. Biomed. Nanotechnol.* **2014**, *10*, 856–863.
- (10) Bray, M.; Di Mascio, M.; de Kok-Mercado, F.; Mollura, D. J.; Jagoda, E. Radiolabeled antiviral drugs and antibodies as virus-specific imaging probes. *Antiviral Res.* **2010**, *88*, 129–142.
- (11) Tao, Y.; Ran, X.; Ren, J.; Xu, X. Array-based sensing of proteins and bacteria by using multiple luminescent nanodots as fluorescent probes. *Small* **2014**, *10*, 3667–3671.
- (12) Xu, W.; Krishnakumar, S.; Miranda, M.; Jensen, M. A.; Fukushima, M.; Palm, C.; Fung, E.; Davis, R. W.; St; Onge, R. P.; Hyman, R. W. Targeted and highly multiplexed detection of microorganisms by employing an ensemble of molecular probes. *Appl. Environ. Microbiol.* **2014**, *80*, 4153–4161.
- (13) Kajimoto, K.; Sato, Y.; Nakamura, T.; Yamada, Y.; Harashima, H. Multifunctional envelope-type nano device for controlled intracellular trafficking and selective targeting in vivo. *J. Controlled Release* **2014**, *190C*, 593–606.
- (14) Peuronen, A.; Forsblom, S.; Lahtinen, M. Sterically controlled self-assembly of tetrahedral M(6)L(4) cages via cationic N-donor ligands. *Chem. Commun.* **2014**, *50*, 5469–5472.
- (15) Li, Y.; Wang, Y.; Huang, G.; Ma, X.; Zhou, K.; Gao, J. Chaotropic-anion-induced supramolecular self-assembly of ionic polymeric micelles. *Angew. Chem., Int. Ed.* **2014**, *53*, 8074–8078.
- (16) Ryder, M. P.; Wu, X.; McKelvey, G. R.; McGuire, J.; Schilke, K. F. Binding interactions of bacterial lipopolysaccharide and the cationic amphiphilic peptides polymyxin B and WLBU2. *Colloids Surf, B* **2014**, *120*, 81–87.
- (17) Wenzel, M.; Chiriac, A. I.; Otto, A.; Zweytick, D.; May, C.; Schumacher, C.; Gust, R.; Albada, H. B.; Penkova, M.; Krämer, U.; Erdmann, R.; Metzler-Nolte, N.; Straus, S. K.; Bremer, E.; Becher, D.; Brötz-Oesterhelt, H.; Sahl, H. G.; Bandow, J. E. Small cationic antimicrobial peptides delocalize peripheral membrane proteins. *Proc. Natl. Acad. Sci. U. S. A.* **2014**, *111*, 1409–1418.
- (18) Melendez-Alafort, L.; Nadali, A.; Pasut, G.; Zangoni, E.; De Caro, R.; Cariolato, L.; Giron, M. C.; Castagliuolo, I.; Veronese, F. M.; Mazzi, U. Detection of sites of infection in mice using ^{99}mTc -labelled PN2S-PEG conjugated to UBI and ^{99}mTc -UBI: a comparative biodistribution study. *Nucl. Med. Biol.* **2009**, *36*, 57–64.
- (19) Saeed, S.; Zafar, J.; Khan, B.; Akhtar, A.; Qureshi, S.; Fatima, S.; Ahmad, N.; Irfanullah, J. Utility of ^{99}mTc -labelled antimicrobial peptide ubiquicidin (29–41) in the diagnosis of diabetic foot infection. *Eur. J. Nucl. Med. Mol. Imaging* **2013**, *40*, 737–743.
- (20) Wu, J. B.; Shao, C.; Li, X.; Shi, C.; Li, Q.; Hu, P.; Chen, Y. T.; Dou, X.; Sahu, D.; Li, W.; Harada, H.; Zhang, Y.; Wang, R.; Zhau, H. E.; Chung, L. W. Near-infrared fluorescence imaging of cancer mediated by tumor hypoxia and HIF1 α /OATPs signaling axis. *Biomaterials* **2014**, *35*, 8175–8185.
- (21) Fischer, C. S.; Baier, M. C.; Mecking, S. Enhanced brightness emission-tuned nanoparticles from heterodifunctional polyfluorene building blocks. *J. Am. Chem. Soc.* **2014**, *135*, 1148–1154.
- (22) Bwambok, D. K.; El-Zahab, B.; Challa, S. K.; Li, M.; Chandler, L.; Baker, G. A.; Warner, I. M. Near-infrared fluorescent nano-GUMBOS for biomedical imaging. *ACS. Nano* **2009**, *3*, 3854–3860.
- (23) Wilson, W. R.; Cockerill, F. R., 3rd. Tetracyclines, chloramphenicol, erythromycin, and clindamycin. *Mayo Clin. Proc.* **1987**, *62*, 906–915.
- (24) Chen, H.; Li, S.; Li, B.; Ren, X.; Li, S.; Mahounga, D. M.; Cui, S.; Gu, Y.; Achilefu, S. Folate-modified gold nanoclusters as near-infrared fluorescent probes for tumor imaging and therapy. *Nanoscale* **2012**, *4*, 6050–6064.
- (25) Chen, H.; Li, B.; Ren, X.; Li, S.; Ma, Y.; Cui, S.; Gu, Y. Multifunctional near-infrared-emitting nano-conjugates based on gold clusters for tumor imaging and therapy. *Biomaterials* **2012**, *33*, 8461–8476.
- (26) Liu, C.; Gu, Y. Noninvasive optical imaging of staphylococcus aureus infection in vivo using an antimicrobial peptide fragment based near-infrared fluorescent probes. *J. Innov. Opt. Health Sci.* **2013**, *6*, 1350026–1350034.
- (27) Tulla-Puche, J.; Auriemma, S.; Falciani, C.; Albericio, F. Orthogonal chemistry for the synthesis of thiocoraline-triostin hybrids. Exploring their structure-activity relationship. *J. Med. Chem.* **2013**, *56*, 5587–5600.
- (28) Boylan, C. J.; Campanale, K.; Iversen, P. W.; Phillips, D. L.; Zeckel, M. L.; Parr, T. R., Jr. Pharmacodynamics of oritavancin (LY333328) in a neutropenic-mouse thigh model of *Staphylococcus aureus* infection. *Antimicrob. Agents Chemother.* **2003**, *47*, 1700–1706.
- (29) Chen, H. Y.; Zhang, X.; Dai, S. H.; Ma, Y.; Cui, S.; Achilefu, S.; Gu, Y. Multifunctional gold nanostar conjugates for tumor imaging and combined photothermal and chemo-therapy. *Theranostics* **2013**, *3*, 633–649.
- (30) Chen, H. Y.; Li, B. W.; Ren, X. Y.; Li, S.; Ma, Y.; Cui, S.; Gu, Y. Multifunctional near-infrared-emitting nano-conjugates based on gold clusters for tumor imaging and therapy. *Biomaterials* **2012**, *33*, 8461–8476.
- (31) Chen, J.; Chen, H. Y.; Cui, S. S.; Xue, B.; Tian, J.; Achilefu, S.; Gu, Y. Glucosamine derivative modified nanostructured lipid carriers for tumor delivery. *J. Mater. Chem.* **2012**, *22*, 5770–5783.
- (32) Ning, X.; Lee, S.; Wang, Z.; Kim, D.; Stubblefield, B.; Gilbert, E.; Murthy, N. Maltodextrin-based imaging probes detect bacteria in vivo with high sensitivity and specificity. *Nat. Mater.* **2011**, *10*, 602–607.
- (33) Van Oosten, M.; Schäfer, T.; Gazendam, J. A.; Ohlsen, K.; Tsompanidou, E.; de Goffau, M. C.; Harmsen, H. J.; Crane, L. M.; Lim, E.; Francis, K. P.; Cheung, L.; Olive, M.; Ntziachristos, V.; van Dijl, J. M.; van Dam, G. M. Real-time in vivo imaging of invasive-and biomaterial-associated bacterial infections using fluorescently labelled vancomycin. *Nat. Commun.* **2013**, *4*, 2584–2591.
- (34) Kong, Y.; Yao, H.; Ren, H.; Subbian, S.; Cirillo, S. L.; Sacchettini, J. C.; Rao, J.; Cirillo, J. D. Imaging tuberculosis with endogenous beta-lactamase reporter enzyme fluorescence in live mice. *Proc. Natl. Acad. Sci. U. S. A.* **2010**, *107*, 12239–12244.
- (35) Chen, H.; Zhang, M.; Li, B.; Chen, D.; Dong, X.; Wang, Y.; Gu, Y. Versatile antimicrobial peptide-based ZnO quantum dots for in vivo bacteria diagnosis and treatment with high specificity. *Biomaterials* **2015**, *53*, 532–544.
- (36) Ferro-Flores, G.; Ocampo-García, B. E.; Melendez-Alafort, L. Development of specific radiopharmaceuticals for infection imaging by targeting infectious micro-organisms. *Curr. Pharm. Des.* **2012**, *18*, 1098–1106.
- (37) Nardini, M.; Dijkstra, B. W. Alpha/beta hydrolase fold enzymes: the family keeps growing. *Curr. Opin. Struct. Biol.* **1999**, *9*, 732–737.
- (38) Payne, D. J.; Gwynn, M. N.; Holmes, D. J.; Pompiano, D. L. Drugs for bad bugs: confronting the challenges of antibacterial discovery. *Nat. Rev. Drug Discov.* **2007**, *6*, 29–40.
- (39) Lu, T. K.; Koeris, M. S. The next generation of bacteriophage therapy. *Curr. Opin. Microbiol.* **2011**, *14*, 24–31.
- (40) Zasloff, M. Antimicrobial peptides of multicellular organisms. *Nature* **2002**, *415*, 89–95.
- (41) Fernebro, J. Fighting bacterial infections-future treatment options. *Drug Resist. Update* **2011**, *14*, 125–139.